

# Complex network view of evolving manifolds

Diamantino C. da Silva,<sup>1</sup> Ginestra Bianconi,<sup>2</sup> Rui A. da Costa,<sup>1</sup> Sergey N. Dorogovtsev,<sup>1,3</sup> and José F. F. Mendes<sup>1</sup>

<sup>1</sup>*Departamento de Física da Universidade de Aveiro & I3N,  
Campus Universitário de Santiago, 3810-193 Aveiro, Portugal*

<sup>2</sup>*School of Mathematical Sciences, Queen Mary University of London, London, E1 4NS, United Kingdom*

<sup>3</sup>*A.F. Ioffe Physico-Technical Institute, 194021 St. Petersburg, Russia*

We study complex networks formed by triangulations and higher-dimensional simplicial complexes representing closed evolving manifolds. In particular, for triangulations, the set of possible transformations of these networks is restricted by the condition that at each step, all the faces must be triangles. Stochastic application of these operations leads to random networks with different architectures. We perform extensive numerical simulations and explore the geometries of growing and equilibrium complex networks generated by these transformations and their local structural properties. This characterization includes the Hausdorff and spectral dimensions of the resulting networks, their degree distributions, and various structural correlations. Our results reveal a rich zoo of architectures and geometries of these networks, some of which appear to be small worlds while others are finite-dimensional with Hausdorff dimension equal or higher than the original dimensionality of their simplices. The range of spectral dimensions of the evolving triangulations turns out to be from about 1.4 to infinity. Our models include simplicial complexes representing manifolds with evolving topologies, for example, an  $h$ -holed torus with progressively growing number of holes. This evolving graph demonstrates features of a small-world network and has a particularly heavy-tailed degree distribution.

## I. INTRODUCTION

In mathematics, engineering, and various fields of natural sciences including, in particular, quantum gravity [1–7], manifolds play a pivotal role. The manifolds are topological spaces locally homeomorphic to Euclidean spaces [8]. Simple examples of manifolds are the circle, the sphere, the torus, etc. The discrete construction of manifolds is by simplices (triangle—2-simplex, tetrahedron—3-simplex, etc.), where a simplex is a building block, and a simplicial complex is homeomorphic to a manifold. The simplicial complex construction is possible for, in particular, any smooth (in other words, differentiable) closed manifold. For example, complexes of triangles (triangulations) are homeomorphic to various surfaces, including the sphere, the torus, etc. Simplicial complexes are extensively treated and used as the discrete version of manifolds [9–12]. One should consciously note the following points. (i) Other discrete versions of manifolds, not based on simplices, are also possible, e.g., various grids. (ii) We consider simplicial complexes constructed of only simplices of equal dimension. (iii) The simplicial complex based discrete description of an arbitrary manifold should include the full set of the edges lengths of the simplices. As is natural, simplicial complexes with all edges equal can represent only a small fraction of manifolds. It was recently proposed to treat simplicial complexes as complex networks formed by the vertices and edges of the simplices [13–18], and so to tackle the problem of evolving manifolds by using apparatus and models taken from the theory of evolving complex networks. This treatment conforms well to the modern interest in properties of networks embedded into various metric spaces [19–21].

The works [13–18] considered simplicial complexes rep-

resenting growing manifolds with a border. Notably, the growth in the evolution models proposed in these papers was wholly due to the attachment of new elements (simplexes or their parts) to the border of a simplicial complex. After the attachment, the resulting part of the simplicial complex did not evolve. Discrete manifolds of dimension  $d$  that are topologically isomorphic to a  $d$ -dimensional sphere, having all their nodes laying on the border, can be simply reduced to  $(d - 1)$ -dimensional manifolds without border topologically isomorphic to a  $(d - 1)$ -dimensional spherical surface as can be seen for instance in the framework of Regge theory [22]. In the present article we explore a large variety of simplicial complexes “triangulating” evolving manifolds, including manifolds with varying topology. In particular, we consider 2-simplicial complexes triangulating surfaces homeomorphic to a sphere and  $h$ -holed (genus- $h$ ) torus with a growing number of holes (genera, in other words). We propose a set of basic complex network models for simplicial complexes representing evolving manifolds without borders, so called closed manifolds. In this evolution, the entire manifold progressively evolves, and any part of it has a chance to be modified at any instant. These manifolds can be growing, equilibrium, and decaying, as particular cases of evolving complex networks [23], and we consider the first two of these cases in detail.

We show that this kind of evolutionary models generate manifolds with a wide spectrum of space dimensions, including different from their original dimensionalities, with a small-world geometry (i.e., infinite-dimensional) only as a particular case. This wide set of different generated Hausdorff dimensions, from 2.5 to  $\infty$ , of our evolving triangulations is in sharp contrast to random planar graphs, which are known to be 4-dimensional typically [1]. It turned out that the range of the spectral

dimensions of these triangulations is from about 1.4 to  $\infty$ . Apart from the emergent dimensions, we describe local structural characteristics of these evolving simplicial complexes, the simplest of which are degree distributions and degree-degree correlations. Advantageously, our models can generate evolving topologies. That is, such networks in different instants of evolution can be not homeomorphic to each other. For example, when implementing our rules of evolution, a sphere can turn into a torus, then into a 2-holed torus, and so on. We describe evolving manifolds homeomorphic to an  $h$ -fold ( $h$ -holed) torus, in which number of such topological features (holes) grows with time, which may be treated as a toy model of the evolving Universe. In our models, the holes emerge with higher probability in places with higher curvature, i.e., near hubs, and, in their turn, while emerging, the holes produce vertices of high degrees, and so increase curvature. In this respect, these topological features are associated with hubs and coevolve.

For demonstration purposes and simplicity, we mostly focus on 2-manifolds, that is, surfaces and their triangulations (2-simplicial complexes). Our conclusions are mainly based on the results of extensive numerical simulations of a set of evolution models of growing and equilibrium simplicial complexes, demonstrating various Hausdorff and spectral dimensions. For growing complexes of two- and higher-dimensional simplexes, we analytically obtain degree distributions.

The paper is organized as follows. For the sake of clarity, Sec. II reminds the basics on triangulations in application to closed surfaces. Section III considers the local transformations of triangulations that keep them within the complete set of triangulations (triangular mesh operations). In Sec. IV we introduce a set of evolution models for simplicial complexes. In Sec. V we describe our findings concerning local features of the resulting simplicial complexes, foremost, their degree distributions. Section VI reveals key metric properties of evolving triangulations, namely emergence of higher space dimensions in these systems and their spectral dimension. Section VII describes evolving simplicial complexes representing manifolds whose topology evolves with time. Finally, in Sec. VIII we discuss our results and their consequences.

## II. TRIANGULATIONS OF CLOSED SURFACES

For the sake of clarity, here we remind a few features of triangulation networks (complexes of triangular faces) representing closed surfaces which are of particular interest in this study. We focus on topological invariants and on a local curvature for such triangulations and the closed surfaces that these specific complexes triangulate. In Section VII, we shall consider an evolution model in which these invariants vary in time.

The absence of a boundary in a surface has two immediate consequences for its triangulations. First, each edge

in such a triangulation has exactly two adjacent triangular faces, and each face has three edges, so we arrive at the following relation between the total number of faces,  $F$ , and the total number of edges,  $E$ :

$$3F = 2E. \quad (1)$$

Let us recall the renowned Euler formula for general polyhedra,

$$\chi = F + N - E. \quad (2)$$

Here  $N$  is the total number of vertices and  $\chi$  is the Euler characteristic, a topological invariant  $\chi = 2(1-h)$ , where  $h$  is the number of holes piercing this polyhedra (genera, in the language of topology). Equally,  $h$  is the number of holes piercing the closed manifold that this polyhedra maps (represents as its discrete version). For a surface homeomorphic to a sphere,  $\chi = 2$ , for a torus,  $\chi = 0$ , and so on. For the  $h$ -holed torus,  $\chi = 2(1-h)$ , and the Betti numbers [9] are  $b_0 = 1$ ,  $b_1 = 2h = 2-\chi$ , and  $b_2 = 1$ . Here the holes in the polyhedra corresponds to the holes in the  $h$ -holed torus that this polyhedra represents. Taking into account Eq. (1), we readily get simple expressions valid for triangulations of closed surfaces:

$$\chi = N - \frac{1}{3}E = N - \frac{1}{2}F. \quad (3)$$

The second consequence of the absence of boundaries is that for any vertex, its vertex degree  $q$  coincides with the number of triangles (triangular faces)  $t$  attached to this vertex,  $q_i = t_i$  for vertex  $i$ . Applying this constraint to the formula for the local curvature  $R_i$  of a triangulation constructed of triangles of equal length

$$R_i = 1 - \frac{1}{2}q_i + \frac{1}{3}t_i, \quad (4)$$

see Refs. [11, 12, 24], gives for the local environment of vertex  $i$  in a closed surface the following local curvature [13]:

$$R_i = 1 - \frac{1}{6}q_i. \quad (5)$$

Thus for such triangulations of closed surfaces, local curvature for any vertex is completely determined by its degree, and in this sense it is a secondary notion here. If the degree is below 6 (i.e.,  $q_i = 3, 4$  or  $5$ ), the local curvature is positive, if above 6, then negative. In triangulations with boundaries, Eq. (5) is violated for vertices on a boundary. The degree of a vertex of this type exceeds the number of triangles attached to the vertex, and an edge on a boundary belongs only to one triangle.

We emphasize that Eqs. (4) and (5) for a local curvature are valid only if all triangular faces in a triangulation network have edges of the same length. The rules of the evolution models in this work do not include edge lengths, and we assume the edge length equality only when treating our results in terms of curvature.

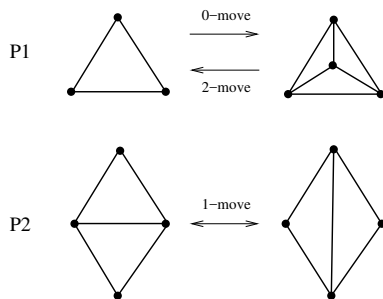


FIG. 1. Pachner moves. The 0-move increases the number of faces by two. The 2 move reduces their number by two.

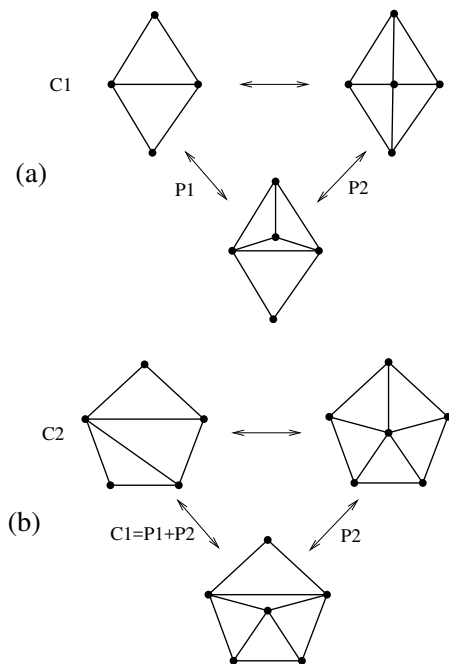


FIG. 2. Examples of transformations that can be reduced to a sequence of Pachner moves. (a) In any of two directions, operation C1 can be performed as a sequence two Pachner moves; from left to right—first P1 and then P2, from right to left—first P2 and then P1. (b) In any of two directions, operation C2 can be performed as a sequence of three Pachner moves.

### III. TRIANGULAR MESH OPERATIONS

Let us introduce transformations, which we use in the next section as elementary steps of the models generating evolving triangulations, and describe relations between these transformations. For triangulations, the evolution rules of our models should satisfy the following conditions. At each step, all the faces must be triangles. It is also demanded that these transformations do not change topological features of the triangulated surface, namely the number of holes (genera) in it. The Pachner moves (bistellar flips) [25–27], Fig. 1, are usually treated to be

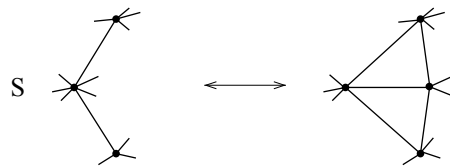


FIG. 3. The “elementary” operation S: splitting–merging of adjacent edges and their joint vertex. The two adjacent edges and their joint vertex are transformed into two adjacent triangles sharing the new edge between the joint vertex and its counterpart. The move from left to right creates two new faces. The move from right to left eliminates two faces. All other faces in this triangulation stay intact. Any triangular mesh transformation can be reduced to a finite sequence of steps, each of which is this operation.

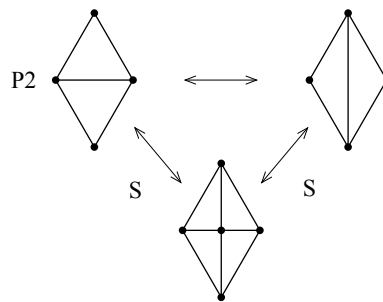


FIG. 4. Pachner move P2 can be performed in two steps by applying S twice.

the minimal necessary set of these “triangular mesh operations”: P1 (the so-called 0-move in one direction, creating a new vertex with three edges within a triangle, and the 2-move in the opposite direction) and P2 (flip of a joint edge between two triangles—the 1-move), in total, three moves. Here we focus on triangulations, but one should note that the Pachner moves are also defined for higher dimensional simplicial complexes [25]. If we consider the closed triangulated 2-dimensional manifold as the boundary of a 3-dimensional manifold formed tetrahedra and isomorphic to a sphere, the Pachner moves can be also interpreted as the result of gluing a single tetrahedra. Specifically the P1 move corresponds to gluing the new tetrahedra to a single triangular face of the boundary of the 3-dimensional manifold, the P2 move corresponds to gluing the new tetrahedra to two incident triangular faces of the 3-dimensional manifold. All other transformations between homeomorphic (topologically equivalent) triangulations can be equivalently performed by a sequence of Pachner moves. Some of such operations were shown in Refs. [28, 29]. For example, the operation C1 shown in Fig. 2(a) can be obtained in two steps by the consecutive application of two Pachner moves, P1 and then P2. Transformations P1 and C1 are called the Alexander moves or star subdivisions [30, 31]. The operation C2 shown in Fig. 2(b) can be obtained in

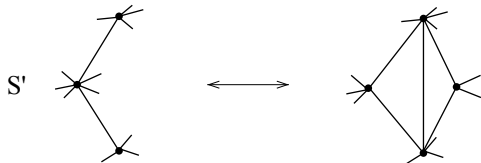


FIG. 5. Operation  $S'$ . In contrast to  $S$  in Fig. 3, the new edge here interconnects the opposite ends of the adjacent edges. Note the following restriction: the adjacent edges on the left cannot belong to the same triangle.

three Pachner steps and so on.

Let us consider now the operation  $S$  explained in Fig. 3, that is splitting of two adjacent edges and the vertex between them in such a way that the vertex and its newborn counterpart are interconnected by a new edge. This operation has two directions—two moves. The Alexander moves  $P1$  and  $C1$  [30, 31] are particular cases of this operation for the situations in which the two split edges belong to the same or two neighboring triangles, respectively. Clearly, this operation can be performed in a finite number of Pachner moves, the same as in the examples shown in Fig. 2. Indeed, operation  $S$  actually coincides with operations of the type shown in Fig. 2. On the other hand, in its turn, each of the Pachner moves can be performed in one or two steps of the operation  $S$ . Indeed, operation  $P1$  is a particular case of operation  $S$ , which means a single application of  $S$ . Further, Fig. 4 demonstrates how Pachner move  $P2$  can be performed in two steps by applying  $S$ .

Note that operation  $S'$  introduced in Fig. 5 (new edge interconnects the opposite ends of the adjacent edges) can be directly obtained from operation  $S$  by Pachner move  $P2$ , and so operation  $S'$  can be performed in a finite number of  $S$  steps. The opposite is, however, not true, although, at first sight, operation  $S'$  looks rather similar to operation  $S$ . The actual reason is that, as Fig. 5 shows, operation  $S'$  is not applicable to a pair of adjacent edges if they belong to the same triangle. That is, operation  $S'$  is possible only in a restricted set of situations and so it in principle cannot be an “elementary triangular mesh operation”.

We conclude that any transformation of triangulation that preserves topology (number of holes in the triangulated surface) can be finally reduced to a sequence of operations  $S$ . So we can reduce the minimal set of triangular mesh operations to the single elementary operation  $S$  (two moves) instead of three Pachner moves.

#### IV. RULES OF EVOLUTION

Our evolution models are organized in the following way. At each time step, (i) an element or neighboring elements of the simplicial complex under consideration are chosen with some preference or, in the simplest partic-

ular case, without preference, i.e., uniformly at random. For triangulations, such elements are vertices, edges, and triangles. Then, (ii) a specific transformation from the set of operations that keep the simplicial complex intact is applied to this element. For triangulations, this transformation is one of the triangular mesh operations, in particular, operations  $P1$ ,  $P2$ ,  $S$ , and  $S'$  described in Sec. IV. Depending on specific (i) and (ii), we get a wide range (zoo) of evolution scenarios, including, in general, growing, decaying, and equilibrium networks with diverse structures, space dimensions, and topologies which we describe in the following sections. We stress the following point. These transformations are interrelated, as we discussed in Sec. IV. Nonetheless, the progressive application of each specific transformation to preferentially selected elements of triangulation networks generates a distinct triangulation.

For the sake of convenience and reference we introduce our models and list them in Table I. This list contains examples for a wide range of situations: equilibrium and growing simplicial complexes, triangulations and higher-dimensional simplicial complexes, and evolving triangulations homeomorphic to closed surfaces with varying in time topology [growing number of holes (genera)]. We choose a set of specific models enabling us to demonstrate a wide spectrum of Hausdorff and spectral dimensions and degree distributions. The problem is that, typically, it is difficult to measure the Hausdorff and spectral dimensions in networks of sizes accessible for our simulations, see Sec. VI. For example, it is virtually impossible to distinguish  $d_H$  equal, say, 20 from  $d_H = \infty$ , valid for small words, since it would demand extremely large, out of reach, network sizes. On the other hand, it is much easier to observe low  $d_H$ , say, 2, 3 or 4 in networks of reasonable sizes. So, for demonstration purposes, we have to choose specific models and their parameters to enable us to observe a set of finite Hausdorff and spectral dimensions for network sizes accessible in our simulations.

Rule  $G1$  and  $G1d$  are describing the same dynamics of the Network Geometry with Flavor [14–17] for  $s = -1, \beta = 0$  and dimension respectively 3 and  $d + 1$ . Specifically the  $G1$  rule is a variation of the random Apollonian graph [32–34] implemented for a 2-simplicial complex triangulating a closed surface.

Rule  $GW$  generates evolving topology, a 2-simplicial complex triangulating an  $h$ -holed torus with a progressively growing number of holes,  $h$ . Each of these holes is created by the merging of a pair of uniformly randomly chosen triangles in a triangulation network. Here the merging of two triangles means that each vertex and edge of one triangle joins the corresponding element of the second triangle forming a single triangle. According to our rule, when this happens, these two faces annihilate, leaving an empty space, namely, a hole after them. We stress that this emergent empty space (triangle of edges without a face) does not belong to the simplicial complex, and so we show it by white color in the scheme for model  $GW$  in Table I. The annihilation of the two merging

faces guarantees that any edge in this complex has two adjacent triangular faces. This transformation changes topology of the underlying closed surface and so, in contrast to the mesh operations in all other of our models, it cannot be reduced to the Pachner moves or operation S. Note that this rule forbids the merging of the nearest-neighbor and, also, second-nearest-neighbor triangles, since this would produce edges laying outside of triangulations, double edges, or 1-cycles. The mergings play a role of a long-range shortcuts in a specific small-world network [35]. Each merging of this kind reduces the Euler characteristic  $\chi$  by 2, resulting in  $\chi = 2(1 - h)$  and the first Betti number  $b_1 = 2h$ . During the evolution, each hole widens with time due to the first channel of the process GW, see Table I. In model GW we do not consider the twisting of the merging triangles. The reason is that any “twisted” configuration can be untwisted by a series of Pachner moves or by applying operation S. This point, however, deserves a more detailed discussion, see Sec. VIII.

We consider long-time asymptotics, which are independent on initial configurations for most of these models. Note, however, that in model E1, the evolution stacks if there is no vertices of degree 3 in a network, and so initial configurations for this case have to contain such vertices. Note also that an initial graph in model GW has to be sufficiently large, since the evolution rule employs merging non-neighbor triangles. As is natural, all initial configurations for our models must be closed manifolds.

## V. LOCAL PROPERTIES

We start considering the local properties of these complex networks with their degree distributions,  $P(k)$ . The degree distributions for the models G1 and G2 of growing triangulations can be derived analytically. For the G1 model for growing triangulations, we write the following rate equation describing the evolution of the average number  $N(k, t) = tP(k, t)$  of vertices of degree  $k$  in the network at time  $t$  (current number of steps):

$$N(k, t + 1) = N(k, t) + 3 \frac{k-1}{\langle k \rangle t} N(k-1, t) - 3 \frac{k}{\langle k \rangle t} N(k, t) + \delta_{k,3}, \quad (6)$$

which directly generalizes the equations for a network growing by attachment of a new vertex to the ends of a randomly chosen edge [36]. Here the average degree of a node,  $\langle k \rangle(t)$ , approaches 6 as  $t \rightarrow \infty$ . The form of the right-hand side of this equation directly follows from the fact that the degree distribution of the vertices of a randomly chosen triangle of a triangulation is  $kP(k)/\langle k \rangle$ . Note that this is the case independently of correlations in the network. In the infinite size, the degree distribution is stationary and independent of initial configuration. (Recall that in this work we consider only closed manifolds, so an initial configuration is also closed.) In this limit,

Eq. (6) is reduced to

$$P(k) = \frac{1}{2}(k-1)P(k-1) - \frac{1}{2}kP(k) + \delta_{k,3}. \quad (7)$$

The solution of this equation is the degree distribution

$$P(k \geq 3) = \frac{24}{k(k+1)(k+2)}, \quad (8)$$

which is in total agreement with the result obtained in [14, 17]. Interestingly also if the network has large clustering coefficient, the obtained degree distribution is exactly the same of the standard Barabási–Albert model [37, 38] in the particular case of attachment of a new vertex to three existing ones. The resulting degree distribution exponent  $\gamma$  equals 3. The degree distribution plot, Fig. 6(a), and the cumulative distribution  $P_{\text{cum}}(k) = \sum_{q=k}^{\infty} P(q)$ , Fig. 6(b), demonstrate that the analytical result completely agrees with numerical simulations. Figure 7(a) showing the average degree  $\langle k \rangle_{\text{nn}}(k)$  of the nearest neighbors of a vertex of degree  $k$ , indicates that the degrees of nearest neighbors in this network are correlated but these correlations are not strong similarly to the Barabási–Albert model (see the region of large  $k$ ). It is natural to consider another type of degree–degree correlations in triangulation networks. Choose an edge uniformly at random. Two triangles share this edge. We consider correlations between the degrees of the two vertices of these triangles that are not ends of this joint edge. These vertices are second nearest neighbors of each other. The point is that they are the closest vertices that belong to different triangles (faces) in this network. In other words, these are two opposite vertices of a rhombus, and there is no edge between them. We characterize these correlations by  $\langle k \rangle_{\text{on}}(k)$  which is the average degree of such neighbors of a vertex of degree  $k$ . Figure 7(b) demonstrates these degree–degree correlations in network G1. Notice that, apart from the region of low  $k$ , these two curves are qualitatively similar to each other despite the stronger separation of vertices in the second case.

The model G2 turns out to be more interesting. Its structure strongly deviates from G1 and the Barabási–Albert model. The rate equations for triangulations growing according to rule G2 have the following form:

$$N(k, t + 1) = N(k, t) + 2 \frac{k-1}{\langle k \rangle t} N(k-1, t) - 2 \frac{k}{\langle k \rangle t} N(k, t) + \delta_{k,4} \quad (9)$$

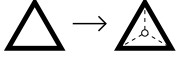
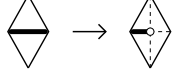
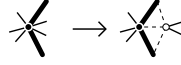
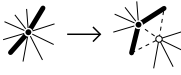
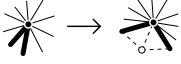
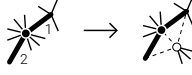
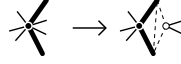
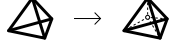
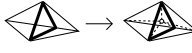
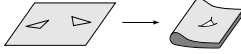
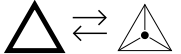
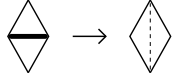
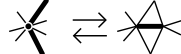
with, similarly to Eq. (6), the mean degree  $\langle k \rangle(t)$  approaching 6 as  $t \rightarrow \infty$ . In this limit, we get

$$P(k) = \frac{1}{3}(k-1)P(k-1) - \frac{1}{3}kP(k) + \delta_{k,4}, \quad (10)$$

and so the degree distribution is

$$P(k \geq 4) = \frac{360}{k(k+1)(k+2)(k+3)}, \quad (11)$$

TABLE I. Zoo of complex network models of evolving closed manifolds

Model	Operation at each step of evolution	Scheme
Growing triangulations		
G1	(i) choose a triangle uniformly at random, (ii) attach a new vertex to all three vertices of this triangle (Pachner's 0-move). (This rule is closely related to the one governing the evolution of random Apollonian networks [32–34]. The difference is that the manifold is closed here.)	
G2	(i) choose an edge uniformly at random, (ii) exchange it for a new vertex attached to all four vertices of the two triangles sharing this edge.	
G	(i) choose a vertex uniformly at random and two its random edges, (ii) split them in the way shown in Fig. 3, the move from left to right.	
Ga	(i) choose a vertex uniformly at random and one of its edges at random; then, among the rest edges of the vertex, if the vertex degree is even, choose the opposite edge to the first, if the degree is odd, choose, with equal probability, one of the two most remote edges (here remote, relatively to the first); (ii) split them in the way shown in Fig. 3, the move from left to right.	
Gb	(i) choose a vertex uniformly at random and one of its edges at random; then, among the rest edges of the vertex, choose, with equal probability, one of the two closest (to the first) edges; (ii) split them in the way shown in Fig. 3, the move from left to right. (Gb is close to rule G1. The difference is that here a random triangle incident to a uniformly chosen vertex is selected.)	
Gc	(i) choose an edge uniformly at random and its end vertex with the highest number of connections (if the degrees of the ends coincide, then choose any one of them with equal probability), (ii) choose the second edge as in rule Ga, (iii) split the two chosen edges and the vertex in the way shown in Fig. 3, the move from left to right.	
G'	(i) choose a vertex uniformly at random and two its random edges except those belonging to the same triangle, (ii) split them in the way shown in Fig. 5, the move from left to right.	
Growing $d$ -dimensional simplicial complexes		
G1d	(i) choose a simplicial complex uniformly at random, and (ii) attach a new vertex to all $d + 1$ vertices of this simplicial complex. (Note that G1d directly generalizes G1 to an arbitrary $d \geq 2$ .)	
G2d	(i) choose a $(d-1)$ -simplex uniformly at random, (ii) attach a new vertex to all $d + 2$ vertices of the two $d$ -simplices sharing the chosen $(d-1)$ -simplex. (Note that G2d is defined only for $d \geq 3$ , and so G2d does not generalize G2 directly.)	
Generation of holes in a growing triangulation		
GW	(i) at each step perform rule G2, and, in addition, (ii) at each $\theta$ -th step choose two triangles, excluding first- and second-neighboring ones, uniformly at random and merge them into a single triangle. These two merging faces annihilate creating a hole (genus) in the triangulation and in the corresponding surface.	
Equilibrium triangulations		
E1	(i) choose a vertex of degree 3 uniformly at random and remove it, (ii) choose a triangle uniformly at random and attach a new vertex to all three vertices of this triangle.	
E2	(i) choose an edge uniformly at random, (ii) perform Pachner 1-move (flip) with this edge (see Fig. 1, P2).	
E3	(i) choose an edge uniformly at random and compress it into one vertex as in transformation S, Fig. 3, the move from left to right, (ii) make a step according to rule G.	

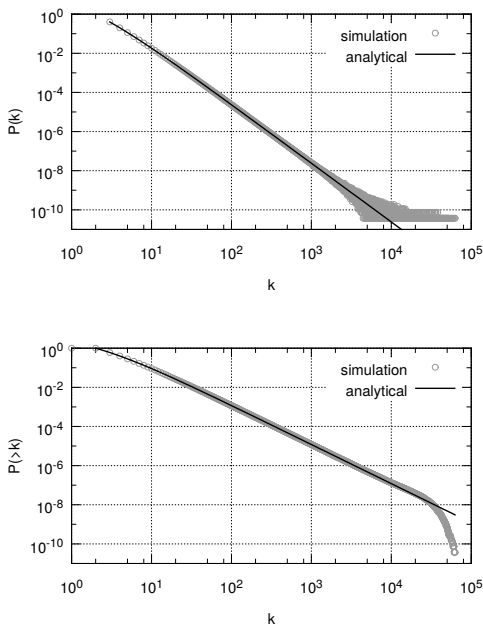


FIG. 6. (a) The degree distribution of model G1: the results of numerical simulations (network of  $2^{27}$  vertices, 200 samples) and the theoretical curve, Eq. (8). (b) The corresponding cumulative degree distribution  $P_{\text{cum}}(k) = \sum_{q \geq k} P(q)$ , simulations and the expression  $12/[k(k+1)]$ , obtained from Eq. (8).

which provides the asymptotics:  $P(k) \sim k^{-4}$ . Consequently, the degree distribution exponent  $\gamma$  equals 4 for this network. Figure 8 validates the analytical results by comparison with numerical simulations. In contrast to G1, this network is essentially correlated as one can see from Fig. 9(a) showing the average degree  $\langle k \rangle_{\text{nn}}(k)$  of the nearest neighbors of a vertex of degree  $k$  in network G2. Notice that these correlations are assortative in the region of large degrees. This is similar to recursive preferentially growing scale-free networks with  $\gamma > 3$ . Figure 9(b) shows the plot of  $\langle k \rangle_{\text{on}}(k)$  for this network. Notice that the second plot indicates at least not weaker degree-degree correlations than in Fig. 9(a), despite the stronger separation of the “on” vertices. Note also that in model G2, the “on” neighbors enter in the evolution rule, which justifies the consideration of these correlations.

We also considered a more complicated mixed model in which at each step rule G1 is realized with probability  $p$  while rule G2 is realized with the complementary probability  $1 - p$ . A straightforward calculation resulted in a power-law degree distribution with the exponent

$$\gamma = 3 + \frac{2(1-p)}{2+p}. \quad (12)$$

The asymptotics of the degree distributions for rules G1 and G2 can be also find for higher-dimensional manifolds. We use the following well-known expression for the degree distribution exponent of scale-free networks

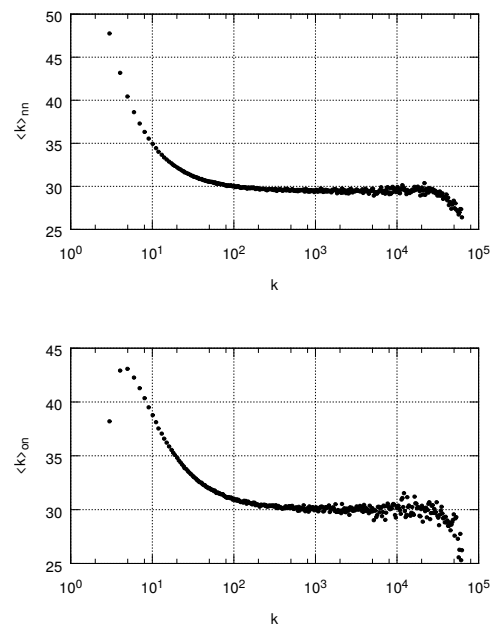


FIG. 7. Degree-degree correlations in model G1. (a) The average degree  $\langle k \rangle_{\text{nn}}(k)$  of the nearest neighbors of a vertex of degree  $k$ . (b) The average degree  $\langle k \rangle_{\text{on}}(k)$  of the vertex in a rhombus, opposite to a vertex of degree  $k$ , that is not its nearest neighbor. The points in the plots are obtained by logarithmic binning the results of numerical simulations for a network of  $2^{27}$  vertices. The numerical simulations employ 200 samples.

growing due to preferential attachment. If the preference function for the probability of attachment to a vertex of degree  $k$  is  $k + A$ , where  $A$  is additional attractiveness, and each new vertex has  $m$  edges, then  $\gamma = 3 + A/m$  [38].

In model G1d, each vertex attains new connections with probability proportional to the number of simplexes incident to this vertex. This number,  $s = s(k, d)$ , is expressed in terms of the degree of a vertex  $k$  and the dimensionality  $d$  of a simplicial complex in the following way:

$$s(k, d) = d + 1 + [k - (d + 1)](d - 1), \quad (13)$$

where  $k \geq d + 1$ . [Notice that, in particular,  $s(k, 2) = k$  for triangulations, and  $s(d + 1, d) = d + 1$ , as is natural.] Consequently, the preference function in model G1d is  $k - (d + 1) + (d + 1)/(d - 1)$ , which leads to

$$\gamma = 2 + \frac{1}{d - 1} \quad (14)$$

since here the number of edges of a new vertex is  $m = d + 1$ . For triangulations ( $d = 2$ ) this confirms the degree distribution exponent  $\gamma = 3$  in model G1, see Eq. (8). According to Eq. (14) exponent  $\gamma$  for model G1d is in the range between 2 ( $d \rightarrow \infty$ ) and 3 ( $d = 2$ ). These results therefore confirm the results obtained in Ref. [14, 15, 17] for manifolds of dimension  $d + 1$  with a boundary.

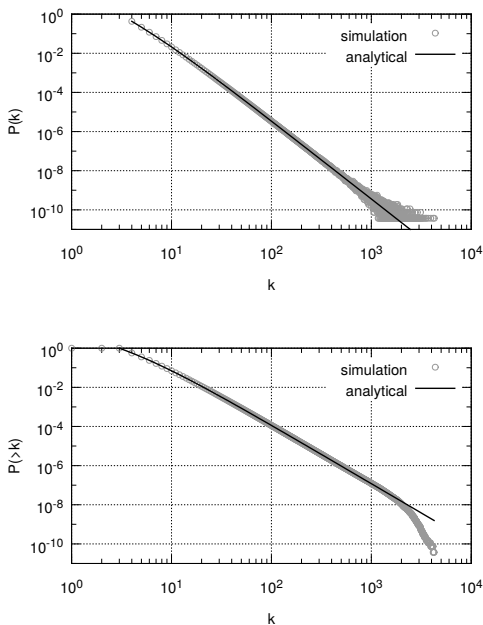


FIG. 8. (a) The degree distribution of model G2: the results of numerical simulations (network of  $2^{27}$  vertices, 200 samples) and the theoretical curve, Eq. (11) (b) The corresponding cumulative degree distribution  $P_{\text{cum}}(k)$ , simulations and the expression  $120/[k(k+1)(k+2)]$ , obtained from Eq. (11).

In contrast to G1d, in our model G2d for ( $d > 2$ )-dimensional growing simplicial complexes, there are actually two kinds of attachment. Of  $d + 2$  edges of a new vertex,  $d$  are attached to the vertices of a randomly chosen ( $d - 1$ )-simplex and the remaining two are attached to the two vertices of the two  $d$ -simplices sharing the ( $d - 1$ )-simplex. It first sight, these two channels principally differ from each other. This is, however, not the case. Let us consider the number  $s_{d-1} = s_{d-1}(k, d)$  of ( $d - 1$ )-simplices incident to a vertex (of degree  $k$ ) in an  $d$ -dimensional simplicial complex and find how this number is related to the number  $s = s(k, d)$  of  $d$ -simplices incident to this vertex, Eq. (13). Each  $d$ -simplex has  $d + 1$  faces [ $(d - 1$ )-simplices], and each of its vertices is on  $d$  of those. Then the number of these faces incident to a vertex is

$$s_{d-1}(k, d) = \frac{d}{2}s(k, d). \quad (15)$$

Here the factor  $1/2$  is due to the fact that each face is shared by a pair of  $d$ -simplices. [Note that when  $d$  is odd, the number  $s(k, d)$  is even, see Eq. (13), which guarantees that  $s_{d-1}(k, d)$  is integer]. Thus, since  $s_{d-1}(k, d)$  is proportional to  $s(k, d)$ , then the preference function for both channels of attachment is the same,  $k - (d+1) + (d+1)/(d-1)$ , as in the G1 model. Now, however, we have  $d + 2$  attachments of a new vertex, so

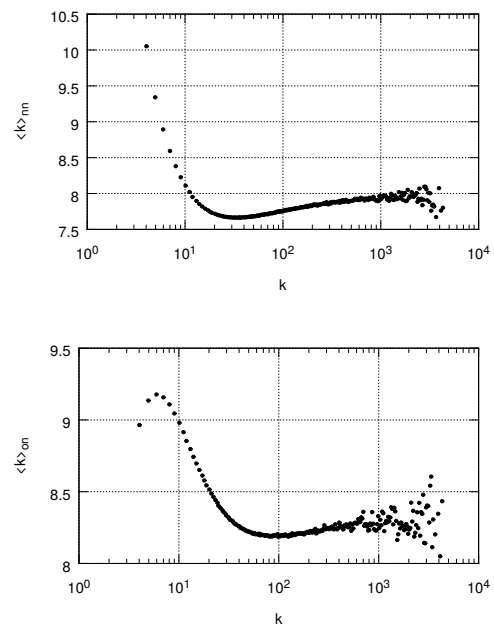


FIG. 9. Degree-degree correlations in model G2. The average degree  $\langle k \rangle_{\text{nn}}(k)$  of the nearest neighbors of a vertex of degree  $k$ . (b) The average degree  $\langle k \rangle_{\text{on}}(k)$  of the vertex in a rhombus, opposite to a vertex of degree  $k$ , that is not its nearest neighbor. The points in the plots are obtained by logarithmic binning the results of numerical simulations for a network of  $2^{27}$  vertices. The numerical simulations employ 200 samples.

we get the degree distribution exponent

$$\gamma = 2 + \frac{2d}{(d-1)(d+2)} \quad (16)$$

for  $d \geq 3$ .

We considered in detail only the power-law distributions. These distributions were generated by models of growing closed manifolds G1 and G2 (growing triangulations) and G1d and G2d. For the other models of growing triangulations discussed in this paper, namely models G, Ga, Gb, Gc, and G', our simulations showed less interesting degree distributions decaying faster than a power law. For our models E1 and E2 of equilibrium triangulations, we reached network sizes of  $2^{17}$ , which turned out to be not sufficient to arrive at a reliable conclusion about the asymptotic form of the degree distributions, though we observed a faster decay than a power law. Simulations of network E3 of this size provided a power-law degree distribution with exponent  $\gamma$  close to 3. We list the resulting degree distribution exponents for our models in Table II, where we indicate  $\infty$  for  $\gamma$  if the corresponding degree distribution decays more rapidly than a power-law function.



## VI. SPACE DIMENSIONS

The key characteristic of the metric structure of a network is its space dimension. For the class of networks considered in this work it coincides with Hausdorff dimension, so we denote it by  $d_H$ . For small worlds, i.e., networks whose diameter increases with size (number of vertices in a network,  $N$ ) slower than a power-law function,  $d_H = \infty$ . There are two main methods to obtain the space dimension: (i) by measuring the asymptotic dependence of the average shortest path distance  $\langle \ell \rangle$  between two uniformly randomly chosen vertices on the network size,  $\langle \ell \rangle \propto N^{1/d_H}$ ; (ii) by measuring the asymptotic dependence of the number of vertices  $V(r)$  within a sphere around a uniformly randomly chosen vertex in a large network on the radius  $r$  of this sphere,  $V(r) \propto r^{d_H}$ . We mostly use the second method as more practical.

For a set of models of growing triangulations, we generated a number of realisations of  $2^{28}$  vertices, and, using them, measured  $V(r)$ , see Fig. 10(a). At first sight, it seems from this figure that all these networks are finite dimensional, since the curves are visually close to a linear dependence in the log-log plot. However, inspecting the logarithmic derivative  $d \ln V(r)/d \ln r$  shows that actually this is the case for only some of these networks, namely for the networks whose dependence  $d \ln V(r)/d \ln r$  has a clear plateau. The difficulty is one needs a huge network to clearly observe a power-law dependence  $V(r)$  in a wide range of  $r$ , say, several orders of magnitude. We observed the following: if we plot this curve for a larger network, this plateau is wider but its height is the same,  $d \ln V(r)/d \ln r|_{\text{plateau}} = d_H$ . On the other hand, if the dependence  $d \ln V(r)/d \ln r$  has a peak instead of a plateau, then we face two possibilities. (i) The peak in this dependence increases with network size  $N$  up to infinity, which means  $d_H = \infty$ . (ii) When  $N$  is greater some value, the height of the peak stops growing while its width proceed increasing, which means that this network is finite dimensional. Consequently, if we observe a peak in the dependence  $d \ln V(r)/d \ln r$  for a given network, then  $d_H$  is certainly greater than its maximum  $d \ln V(r)/d \ln r|_{\text{max}}$ . Based on these considerations, we concluded that our network have space dimensions listed in Table II (in the table we indicate  $d_H = \infty$  when the peak  $d \ln V(r)/d \ln r|_{\text{max}}$  exceeds, say, 10 for our networks of  $2^{28}$  vertices). Note that while space dimension 4 is well known as typical for random planar graphs [1], any other finite value for a random triangulation based network is rather unexpected. Only model Ga has  $d_H$  close to 4. The table shows that while the models (G1, G2, GW) with small degree distribution exponent  $\gamma$  have high or even infinite  $d_H$ , which is natural, the high or infinite  $\gamma$  may be associated both with finite  $d_H$  (models Ga and Gc) and with large or infinite  $d_H$  (models G and Gb). The equilibrium networks E1, E2, and E3 that we generated in our numerical simulations were not sufficiently large to obtain  $d_H$  confidently, so we have to leave three empty spaces in the table.

Another key characteristic of the large scale organisation of a network is its spectral dimension  $d_S$ , which, in simple terms, is its space dimension measured by using a diffusion process. For this process, the large time asymptotics of the density distribution at the starting vertex at time  $t$  is

$$p_0(t) \sim t^{-d_S/2} \quad (17)$$

for an infinite network. This corresponds to the following density of states of the Laplacian spectrum

$$\rho(\lambda) \sim \lambda^{d_S/2-1} \quad (18)$$

for small eigenvalues  $\lambda$ . In finite networks, the dependence  $p_0(t)$  has an exponential cutoff corresponding to the gap between the eigenvalue 0 and the first nonzero eigenvalue of the Laplacian spectrum. For obtaining  $d_S$  we inspected the number of (nonzero) eigenvalues in the Laplacian spectra smaller than  $\lambda$ ,  $N_{<}(\lambda) = \sum_{i: 0 < \lambda_i \leq \lambda} 1$ , which is proportional to the cumulative density of states of the Laplacian spectra (has  $N$  eigenvalues), see Fig. 11. To reduce fluctuations, which are large for small eigenvalues, we averaged eigenvalue  $\lambda_i$  for each given  $i$  over samples before calculating the cumulative numbers  $N_{<}(\lambda)$ . For each model we obtained a set of smallest eigenvalues of its Laplacian spectrum since only they were needed to find  $d_S$ . The curves in Fig. 11 reach the value  $N - 1$  at large  $\lambda$ . The log-log plots in this figure provide the set of values of  $d_S$  presented in Table II. These resulting numbers differ strongly from the Hausdorff dimensions of these triangulation based networks and sit in the region from 1.4(2) for E1 to 2.9(2) for G1. As one could expect, this region includes dimension 2 of the simplex (triangle), although the observed deviations from this value are marked. Notice also that in these networks the spectral dimensions  $d_S$  are finite even when  $d_H$  is infinite, i.e., when they are small worlds. We shall suggest however based on our simulations in Sec. VII that the small-world network GW (model generating which play the role of long-range shortcuts) has its spectral dimension  $d_S = \infty$  the same as  $d_H$ . The rest growing networks in Table II have  $d_H > d_S$ .

Notice the spectral dimension  $d_S = 1.4(3)$  for model E1. As we mentioned above, we did not obtain its Hausdorff dimension. We expect however that  $d_H$  for this network is close to 2. Interestingly, a similar combination of dimensions is valid for the ensemble of random connected trees (i.e., each member of the ensemble consists of a single connected component), in which  $d_H = 2$  and  $d_S = 4/3$  [39–42].

## VII. GENERATION OF HOLES: EVOLVING TOPOLOGY

The closed manifolds considered above stayed homeomorphic to a sphere (or hypersphere) during the entire evolution. In contrast to these models, model GW from

TABLE II. Key characteristics of network models of closed triangulations: exponent  $\gamma$  of a degree distribution  $P(k) \sim k^{-\gamma}$ , Hausdorff dimension  $d_H$ , and spectral dimension  $d_S$ . The values of  $\gamma$  for models G1 and G2 are exact, the other numbers in the table were obtained from simulations. The simulated in this work networks E1, E2, and E3 were too small to obtain their Hausdorff dimensions.

model	exponent $\gamma$	Hausdorff dimension $d_H$	spectral dimension $d_S$
Growing triangulations			
G1	3	$\infty$	2.9(2)
G2	4	$>5.7$	2.4(2)
G	$\infty$	$>5.0$	2.0(3)
Ga	$\infty$	3.8(2)	2.0(4)
Gb	$>4.5$	$\infty$	2.4(3)
Gc	$\infty$	2.6(2)	2.0(3)
Growing triangulation with increasing number of holes			
GW	$\lesssim 2.0$	$\infty$	$\gtrsim 14$
Equilibrium triangulations			
E1	$\infty$	—	1.4(2)
E2	$\infty$	—	1.9(4)
E3	3.0(2)	—	2.1(2)

Table I generates networks triangulating manifolds with evolving topology. In this model two processes are applied in parallel. (i) At each step, the same move as in model G2 is made. (ii) In addition, at each  $\theta$ -th step, merging of two randomly chosen triangles (and annihilating these two faces as explained in Sec. IV) produces a hole (genus) in this manifold. The number of vertices in this network is  $t(1 - 3/\theta)$  asymptotically. As a result we have an  $h$ -holed torus with a progressively growing number  $h \cong t/\theta$  of holes. Model GW reduces to model G2 in the limit  $\theta \rightarrow \infty$ .

Figure 12 demonstrates the degree distributions and the cumulative degree distributions of the manifolds evolving according to rule GW. The results were obtained by numerical simulations in which the networks were grown up to  $2^{20}$  vertices for a set of periods  $\theta$ , from 10 to  $\infty$ . As is natural, for  $\theta \rightarrow \infty$  we observe a power-law degree distribution of model G2, with exponent  $\gamma = 4$ . For finite  $\theta$ , the degree distribution in the region of large degrees decays slower than in model G2. As  $\theta$  decreases, this slow decay becomes observable at lower degrees, and it can be roughly estimated as  $\sim k^{-2}$  or even slower.

It is worthwhile to note that model GW is essentially similar to the aggregation growing network [43] (model D in the cited work) in which, at each step, the end vertices of a uniformly randomly chosen edge merged together. The resulting aggregation process in Ref. [43] was treated analytically. It was found that the network has a particularly slowly decaying degree distribution and, in a wide region of parameters, demonstrates a condensation phenomenon (a single vertex attracts a finite fraction of all connections). This is why the slowly decaying degree

distributions of networks GW in Fig. 12 are not surprising. However, in contrast to Ref. [43], we did not observe condensation phenomena in model GW. One of possible reasons for that is the additional constraint that forbids merging first- and second- nearest-neighboring triangles. This also makes an analytical treatment of the model more challenging than in Ref. [43].

In model GW, hubs preferentially (proportionally to degree, i.e., local curvature) participate in emergence of holes. On the other hand, the birth of a hole produces vertices of higher degrees. So hubs and holes co-evolve and strongly correlate with each other. Furthermore, for sufficiently small values of the merging period  $\theta$ , in particular for  $\theta = 10$ , we observed that in a fraction of runs, the evolution process GW stalled during the observation time, which was about  $10^6$  steps, and we had to restart the process from zero. The reason for this stall is that this network is so compact (the average separation of vertices approaches only 4 at  $t \sim 10^6$ , see Fig. 13) that it is possible that at some instant our algorithm cannot find triangles relevant for merging. (Recall that they cannot be first- and second-nearest neighbors by the rules of the model).

To characterise long-range properties of these manifolds we inspected the evolution of the average distance,  $\langle \ell \rangle$ , between vertices of the generated networks for different values of parameter  $\theta$ , see Fig. 13. The curve for  $\theta = \infty$  increases with  $t$  in this range,  $1 \leq t \leq 10^6$ , faster than the first power of logarithm. Our more thorough analysis in Sec. VI showed that network G2 has very large, probably infinite, dimension  $d_H$ . In this sense, network G2 already can be called a “small world”. Nonethe-

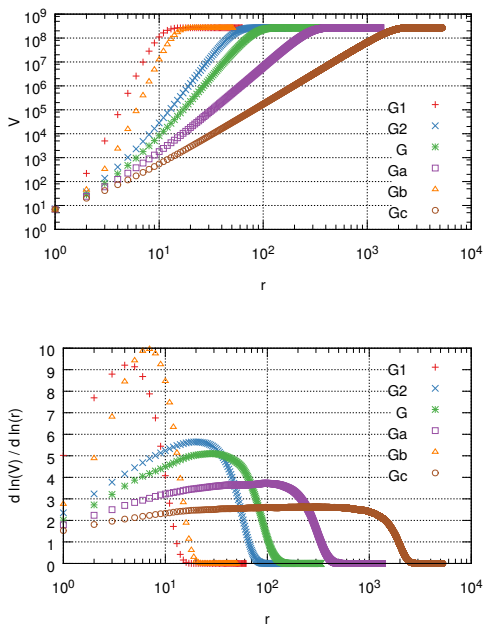


FIG. 10. (a) The average number of vertices,  $V(r)$ , at a distance  $r$  or smaller from a randomly chosen vertex as a function of  $r$  for the models G, G2, Ga, Gb, and Gc of growing triangulation networks. (b) The logarithmic derivative  $d \ln V(r) / d \ln r$ . The presence of a plateau on a curve for the logarithmic derivative indicates that the corresponding network is finite-dimensional. The networks in the numerical simulations are of  $2^{28}$  vertices. The sizes of samples in the simulations for models G, Ga, Gb, and Gc are 16, 24, 16, and 16, respectively. For each sample, 100 vertices are chosen uniformly at random, around which the spheres of radius  $r$  are made.

less, as Fig. 13 demonstrates, the additional merging of triangles during the evolution produces a particularly strong small-world effect, i.e., the network becomes even more compact. For  $\theta < 1000$ ,  $\langle \ell \rangle$  increases with  $t$  even slower than the first power of logarithm. The emerging holes play the role of shortcuts between random vertices of the Watts-Strogatz model of a small-world network [35] but applied not to a one-dimensional lattice, as in the original model, but to a very high-dimensional or even infinite-dimensional network. So, according to Fig. 13, we may arrive even at so-called “ultra-small worlds” [44, 45].

Finally we investigated the Laplacian spectrum of model GW to obtain its spectral dimension  $d_S$ . Figure 14, showing the cumulative Laplacian spectra of the networks with different  $\theta$ , demonstrate that  $d_S$  is very high if not infinite. For example, for the network with  $\theta = 10$ , see Figs. 11 and 14, we observe the slope about 14 of the curve in the log-log plot for small  $\lambda$ . Interestingly, in Fig. 14, this slope saturates as period  $\theta$  becomes smaller than 200. However, the region of  $\lambda$ , where this power-law asymptotic is observed, is very narrow. We suggest that this slope (and the value of  $d_S$ ) should be

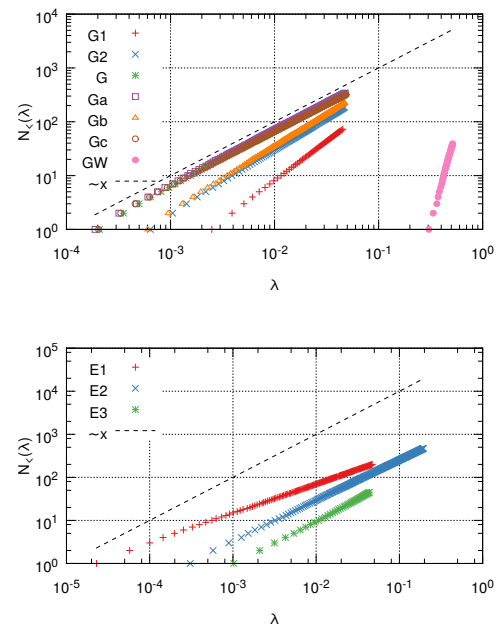


FIG. 11. (a) Cumulative number of Laplacian spectrum eigenvalues,  $N_<(\lambda) = \sum_{i: 0 < \lambda_i \leq \lambda} 1$ , for the models G1, G2, G, Ga, Gb, Gc, and GW of growing triangulation networks. The spectra are obtained for the networks of  $2^{17}$  vertices. The results are accumulated from 639, 256, 64, 32, 64, 32, and 32 samples for models G1, G2, G, Ga, Gb, Gc, and GW respectively. (b) Cumulative number of Laplacian spectrum eigenvalues for the models E1, E2, and E3 of equilibrium triangulation networks. The spectra are obtained for the networks of  $2^{15}$  vertices. For each model, the results are accumulated from 32 samples. The dashed lines have the slope 1, corresponding to the Laplacian dimension  $d_L = 2$ .

even infinite for the infinite networks generated by this model. The difficulty is that the investigated networks are rather small,  $10^4$ – $10^5$  vertices, and, what is even more important, are very compact, the mean separation of vertices is about 4 when  $\theta = 10$ , while the size effect is strong, see Fig. 15 showing the dependencies  $N_<(\lambda)$  at  $\theta = 200$  for different network sizes  $N$ . This figure demonstrates that the slope of the cumulative Laplacian spectrum in the region of small  $\lambda$  increases with network size. For a fixed  $\theta$ , the number of holes–shortcuts is proportional to the network size. So this plot also describes the effect of shortcuts on the Laplacian spectrum of this specific growing small-world network. Notice that for the cumulative density of states in the Laplacian spectrum,  $N_<(\lambda)/N$ , the curves obtained from Fig. 15 practically coincide with each other in the respective regions of  $\lambda$ , see the inset of Fig. 15.

## VIII. DISCUSSIONS AND CONCLUSIONS

We did not consider some issues related to an interplay between topology, metric structure, and the non-

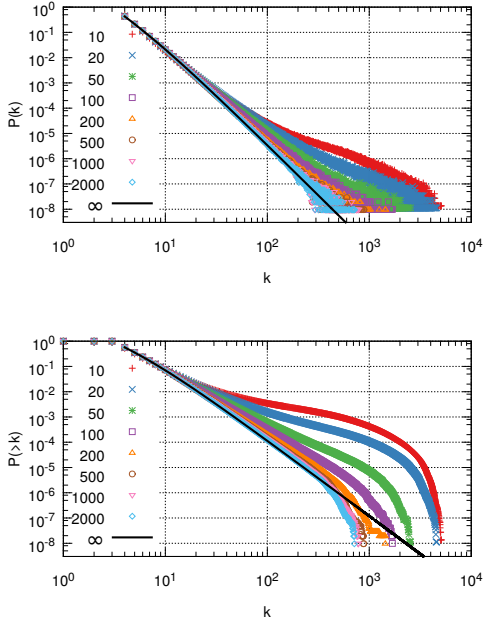


FIG. 12. (a) Degree distribution of the model GW of a growing triangulation network with periodically merging triangles ( $h$ -holed torus). Different periods  $\theta$  for introducing the holes are considered,  $\theta=10, 20, 50, 100, 200, 500, 1000, 2000$ , and  $\infty$ . The resulting networks in the numerical simulations are of  $2^{20}$  vertices, the averaging is over 10 (for  $\theta = 10$ ) or 100 (for  $\theta \geq 20$ ) samples. The infinite period  $\theta$  provides model G2. (b) The corresponding cumulative degree distributions.

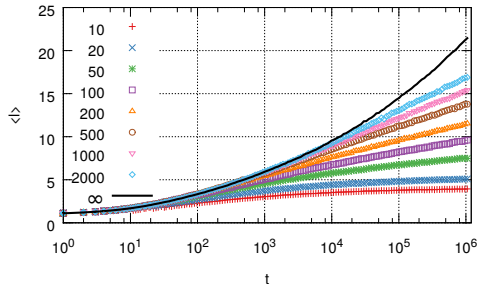


FIG. 13. The time evolution of the average distance between vertices in the model GW of a growing triangulation network with periodically merging triangles. Different curves are obtained for different periods  $\theta$  of introducing the holes,  $\theta=10, 20, 50, 100, 200, 500, 1000, 2000$ , and  $\infty$ . The curve for  $\theta \rightarrow \infty$  corresponds to model G2.

equilibrium nature of many of our evolution models. One of these interesting issues is possible twisting of merging triangles. This twisting would mean that the shortest path between two points may spiral around a hole, i.e., it relates to a metric structure. We did not consider this twisting in Sec. IV since a (long) sequence of Pachner moves (or operation S from Sec. III) can smoothly untwist the configuration of this kind. This possibil-

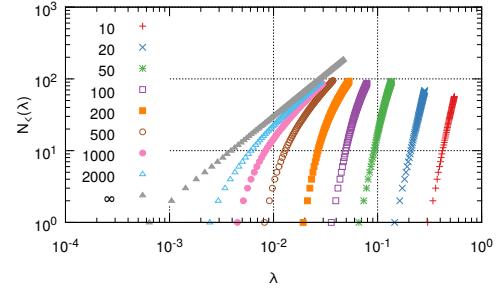


FIG. 14. Cumulative number of Laplacian spectrum eigenvalues of model GW for a set of values  $\theta=10, 20, 50, 100, 200, 500, 1000, 2000$ , and  $\infty$ . The network size is  $2^{17}$  vertices.

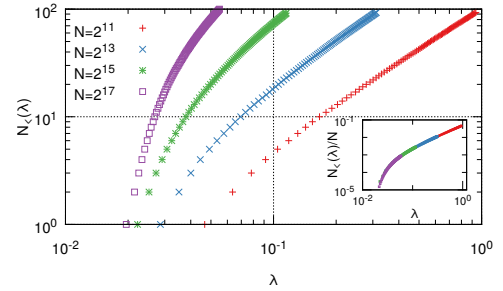


FIG. 15. Cumulative number of Laplacian spectrum eigenvalues of model GW,  $\theta=200$ , for a set of network sizes. The inset shows the cumulative density of the Laplacian spectrum  $N_{<math>(<\lambda)/N</math> vs  $\lambda$  for the same set of network sizes. Notice that all the curves in the inset precisely coincide in the respective regions of  $\lambda$ .$

ity of untwisting should be typical for equilibrium models, but the situation may be more complicated for non-equilibrium networks of this kind. Indeed, if we introduce twisting for each of the frequently occurring mergings into a growing network of the GW kind, then the second channel of the evolution process will have no time to complete untwisting. Analysis of the interesting resulting object is beyond the scope of the present work.

We explained that for precise measuring space dimensions of our objects one should simulate a very large networks. More extensive simulations than in this work can provide  $d_H$  values even for our equilibrium models, for which we succeed to reach only sizes of  $10^5$  vertices, not sufficient to obtain  $d_H$ .

We derived analytical expressions for degree distributions of a few our models. We suggest that an analytical, at least approximate, theory of a much wider range of these models is, in principle, doable, in particular for model GW, following ideas from Ref. [43]. Furthermore, the rules of our evolution models do not specify edge lengths. We leave more detailed models for simplicial complexes with edges of different length for future work.

It is worthwhile to mention that in the complex net-

works literature the term “network topology” is interpreted frequently as a structural organization, a global structure, and so on. In contrast to this, in the present article we treat this term in the standard mathematical sense and consider the full set of topological features of our systems.

The zoo of networks that we considered is just the tip of the iceberg. We focused on evolution processes not related to boundaries. However merging of simplices and generation of holes can be considered not only in closed manifolds, as in Sec. VII, but also in manifolds with boundaries. Moreover, the number of boundaries can also be evolving, new boundaries can be generated progressively. Other promising generalizations and variations of our models are also possible. In particular, if instead of the annihilation of two merging faces in the rules of model GW, we introduce merging two triangular faces into one, we shall obtain an expanding foam.

We found that the constraint that a network is a triangulation produces a strong difference from typical planar graphs, random geometric graphs, and other networks embedded in metric spaces [1, 46–48]. This difference lays beyond such local characteristics as degree distributions. Our models provide a rich array of dimensions of generated metric spaces and evolving topologies with varying set of topological features. We obtained a wide spectrum of Hausdorff and spectral dimensions for our models of evolving triangulations. Notably, for some of them,  $d_H$  is infinite, while  $d_S$  is finite, see Table II. In this situation, diffusion processes on a network look like

in a finite-dimensional metric space despite the extremal compactness of the network.

We observed that “physical” stochastic network models used for interpretation of evolving simplicial complexes produce a set of surprising results for their local properties (heavy tailed degree distributions) and global ones (unusual values of space dimensions, topological features, holes, coupled with high local curvature). These effects combine the evolution, topology, and geometry of the considered objects. Although our conclusions are made for abstract mathematical structures, we suggest that more detailed versions of our models and algorithms could be applied to real-world systems and processes. Triangulations are in the very heart of modern civilization providing the main method of treatment of surfaces in topography, engineering, hydrodynamics and aerodynamics, visualization techniques, and everywhere. We suggest that an important application of our work could be development of efficient stochastic algorithms generating triangulations and higher-dimensional simplicial complexes with desired characteristics and features.

## ACKNOWLEDGMENTS

D. C. S. was supported by the grant FEDER No. POCI-01-0145-FEDER-007688. R. A. C. acknowledges the grants BPD-35/I3N/SET2016/21537 and FCT SFRH/BPD/123077/2016.

- 
- [1] J. Ambjørn and B. Durhuus, *Quantum Geometry: A Statistical Field Theory Approach* (Cambridge University Press, Cambridge, 1997).
- [2] J. Ambjørn, M. Carfora, and A. Marzuoli, *The Geometry of Dynamical Triangulations* (Springer, Berlin, 1997).
- [3] C. Rovelli and F. Vidotto, *Covariant Loop Quantum Gravity: An Elementary Introduction to Quantum Gravity and Spinfoam Theory* (Cambridge University Press, Cambridge, 2014).
- [4] J. C. Baez, “An introduction to spin foam models of bf theory and quantum gravity,” *Lect. Notes Phys.* **543**, 25 (2000).
- [5] J. Ambjørn, J. Jurkiewicz, and R. Loll, “Quantum gravity as sum over spacetimes,” *Lect. Notes Phys.* **807**, 59 (2010).
- [6] J. Lombard, “Network gravity,” arXiv preprint arXiv:1602.04220 (2016).
- [7] B. Krüger, *Simulating Triangulations: Graphs, Manifolds and (Quantum) Spacetime* (FAU University Press, Boca Raton, 2016).
- [8] H. Edelsbrunner and J. Harer, *Computational Topology: An Introduction* (American Mathematical Society, Providence, 2010).
- [9] J. R. Munkres, *Elements of Algebraic Topology* (Addison-Wesley, Redwood City, 1984).
- [10] T. Y. Kong and A. Rosenfeld, “Digital topology: Introduction and survey,” *Computer Vision, Graphics, and Image Processing* **48**, 357 (1989).
- [11] Y. Higuchi, “Combinatorial curvature for planar graphs,” *J. Graph Theor.* **38**, 220 (2001).
- [12] M. Keller, “Curvature, geometry and spectral properties of planar graphs,” *Discrete & Computational Geometry* **46**, 500 (2011).
- [13] Z. Wu, G. Menichetti, C. Rahmede, and G. Bianconi, “Emergent complex network geometry,” *Sci. Rep.* **5**, 10073 (2015).
- [14] G. Bianconi, C. Rahmede, and Z. Wu, “Complex quantum network geometries: Evolution and phase transitions,” *Phys. Rev. E* **92**, 022815 (2015).
- [15] G. Bianconi and C. Rahmede, “Complex quantum network manifolds in dimension  $d > 2$  are scale-free,” *Sci. Rep.* **5**, 13979 (2015).
- [16] G. Bianconi and C. Rahmede, “Emergent hyperbolic geometry of growing simplicial complexes,” arXiv preprint arXiv:1607.05710 (2016).
- [17] G. Bianconi and C. Rahmede, “Network geometry with flavor: from complexity to quantum geometry,” *Phys. Rev. E* **93**, 032315 (2016).
- [18] O. T. Courtney and G. Bianconi, “Generalized network structures: The configuration model and the canonical ensemble of simplicial complexes,” arXiv preprint arXiv:1602.04110 (2016).
- [19] F. Papadopoulos, M. Kitsak, M. Á. Serrano, M. Boguñá, and D. Krioukov, “Popularity versus similarity in grow-

- ing networks,” *Nature* **489**, 537 (2012).
- [20] K. Zuev, O. Eisenberg, and D. Krioukov, “Exponential random simplicial complexes,” *J. Phys. A: Mathematical and Theoretical* **48**, 465002 (2015).
- [21] D. Krioukov, “Clustering implies geometry in networks,” *Phys. Rev. Lett.* **116**, 208302 (2016).
- [22] B. Dittrich and P. A. Höhn, “Canonical simplicial gravity,” *Classical and Quantum Gravity* **29**, 115009 (2012).
- [23] S. N. Dorogovtsev and J. F. F. Mendes, “Scaling behaviour of developing and decaying networks,” *EPL (Europhysics Letters)* **52**, 33 (2000).
- [24] O. Knill, “On index expectation and curvature for networks,” arXiv preprint arXiv:1202.4514 (2012).
- [25] U. Pachner, “PL homeomorphic manifolds are equivalent by elementary shellings,” *Eur. J. Combinatorics* **12**, 129 (1991).
- [26] A. Björner and F. H. Lutz, “Simplicial manifolds, bistellar flips and a 16-vertex triangulation of the poincaré homology 3-sphere,” *Experimental Mathematics* **9**, 275 (2000).
- [27] C. Cortés, C. Grima, A. Marquez, and A. Nakamoto, “Diagonal flips in outer-triangulations on closed surfaces,” *Discrete mathematics* **254**, 63 (2002).
- [28] C. Loop, *Managing adjacency in triangular meshes*, Tech. Rep. (Tech. rep. No. MSR-TR-2000-24, Microsoft Research, 2000, <http://research.microsoft.com/en-us/um/people/cloop/msrtr-2000-24.pdf>).
- [29] I. Izmetiev, S. Klee, and I. Novik, “Simplicial moves on balanced complexes,” arXiv preprint arXiv:1512.04384 (2015).
- [30] T. Aste, “Dynamical partitions of space in any dimension,” *J. Physics A: Mathematical and General* **31**, 8577 (1998).
- [31] B. Dittrich and M. Geiller, “Flux formulation of loop quantum gravity: Classical framework,” *Classical and Quantum Gravity* **32**, 135016 (2015).
- [32] T. Zhou, G. Yan, P.-L. Zhou, Z.-Q. Fu, and B.-H. Wang, “Random apollonian networks,” arXiv preprint cond-mat/0409414 (2004).
- [33] Z. Zhang, L. Rong, and F. Comellas, “High-dimensional random apollonian networks,” *Physica A* **364**, 610 (2006).
- [34] A. Frieze and C. E. Tsourakakis, “On certain properties of random apollonian networks,” in *International Workshop on Algorithms and Models for the Web-Graph* (Springer, 2012) p. 93.
- [35] D. J. Watts and S. H. Strogatz, “Collective dynamics of small-world networks,” *Nature* **393**, 440 (1998).
- [36] S. N. Dorogovtsev, J. F. F. Mendes, and A. N. Samukhin, “Size-dependent degree distribution of a scale-free growing network,” *Phys. Rev. E* **63**, 062101 (2001).
- [37] A.-L. Barabási and R. Albert, “Emergence of scaling in random networks,” *Science* **286**, 509 (1999).
- [38] S. N. Dorogovtsev, J. F. F. Mendes, and A. N. Samukhin, “Structure of growing networks with preferential linking,” *Phys. Rev. Lett.* **85**, 4633 (2000).
- [39] R. Rammal and G. Toulouse, “Random walks on fractal structures and percolation clusters,” *J. Physique Lett.* **44**, 13 (1983).
- [40] T. Jonsson and J. F. Wheeler, “The spectral dimension of the branched polymer phase of two-dimensional quantum gravity,” *Nucl. Phys. B* **515**, 549 (1998).
- [41] B. Durhuus, “Hausdorff and spectral dimension of infinite random graphs,” *Acta Phys. Polon.* **40**, 3509 (2009).
- [42] J. Wheeler, *Gravity, random graphs and spectral dimension*, Tech. Rep. (2009, <https://www.kent.ac.uk/smsas/personal/tcd/webpages/icft10/wheater.pdf>).
- [43] M. J. Alava and S. N. Dorogovtsev, “Complex networks created by aggregation,” *Phys. Rev. E* **71**, 036107 (2005).
- [44] R. Cohen and S. Havlin, “Ultra small world in scale-free networks,” *Phys. Rev. Lett.* **90**, 058701 (2002).
- [45] S. N. Dorogovtsev, J. F. F. Mendes, and A. N. Samukhin, “Metric structure of random networks,” *Nucl. Phys. B* **653**, 307 (2003).
- [46] M. Penrose, *Random Geometric Graphs* (Oxford University Press, Oxford, 2003).
- [47] J. Dall and M. Christensen, “Random geometric graphs,” *Phys. Rev. E* **66**, 016121 (2002).
- [48] L. Daqing, K. Kosmidis, A. Bunde, and S. Havlin, “Dimension of spatially embedded networks,” *Nature Phys.* **7**, 481 (2011).